

Digital mapping of coffee ripeness using UAV-based multispectral imagery



Rodrigo Nogueira Martins ^{a,d,*}, Francisco de Assis de Carvalho Pinto ^a, Daniel Marçal de Queiroz ^a, Domingos Sárvio Magalhães Valente ^a, Jorge Tadeu Fim Rosas ^b, Marcelo Fagundes Portes ^a, Elder Sânzio Aguiar Cerqueira ^c

^a Department of Agricultural Engineering, Universidade Federal de Viçosa (UFV), Viçosa, Brazil

^b Department of Soil and Plant Nutrition, Universidade de São Paulo (USP-ESALQ), Piracicaba, Brazil

^c Department of Geotechnics and Transportation, Universidade Federal de Juiz de Fora (UFJF), Juiz de Fora, Brazil

^d Instituto Federal do Norte de Minas Gerais (IFNMG), Araçuaí, Brazil

ARTICLE INFO

Keywords:

Fruit ripeness
Drone
Digital agriculture
Remote sensing
Random forest

ABSTRACT

Timely and accurate monitoring of coffee ripeness is essential for harvest planning, especially in mountainous areas where the harvest is performed manually due to the limited use of agricultural mechanization. The increasing temporal and spatial resolutions of remote sensing based on low-altitude unmanned aerial vehicles (UAV) provides a feasible way to monitor the fruit ripeness variability. Due to these facts, this study was aimed to: (1) predict the fruit ripeness using spectral and textural variables; and (2) to determine the best variables for developing spatio-temporal variability maps of the fruit ripeness. To do so, an experiment with six arabica coffee fields was set up. During the coffee ripeness stage in the 2018–2019 and 2020–2021 seasons, seven flights were carried out using a quadcopter equipped with a five-band multispectral camera. After that, 12 spectral and 64 textural variables composed of bands and vegetation indices were obtained. For the same period, the percentage of unripe fruits (fruit ripeness) was determined using an irregular grid on each field. Then, the fruit ripeness was predicted with six machine learning (ML) algorithms using as input (1) the spectral variables and (2) the combination of spectral and textural variables. Among the evaluated ML algorithms, the random forest presented the higher accuracy, in which the model using the spectral and textural variables ($r^2 = 0.71$ and RMSE = 11.47%) presented superior performance than the model based solely on spectral variables ($r^2 = 0.67$ and RMSE = 12.09%). Finally, this study demonstrated the feasibility of using spectral and textural variables derived from UAV imagery for mapping and monitoring the spatiotemporal changes in the fruit ripeness at a fine scale.

1. Introduction

Coffee is one of the three major beverages consumed worldwide whose economic value is defined according to its quality, which in turn is affected by many characteristics (Silva et al., 2014, 2017). One of the most important is the fruit ripeness at harvest. Ripe fruits provide a better quality coffee, while unripe and overripe fruits reduce its quality (Martinez et al., 2013; Silva et al., 2014). Because of that, the fruit ripeness is a key parameter for defining the moment of starting the harvest, especially for farmers that want to reach higher beverage quality.

Currently, the fruit ripeness monitoring is carried out periodically through repeated manual counts of ripe fruits made on a few plants within each field (Nogueira Martins et al., 2021). To avoid the

traditional field monitoring, which is time-consuming, labor-intensive, and not fully representative, a few studies were conducted throughout the years using vegetation indices (VI) derived from unmanned aerial vehicle (UAV) imagery (Herwitz et al., 2004; Johnson et al., 2004; Nogueira Martins et al., 2021; Rosas et al., 2021).

The studies conducted by Herwitz et al. (2004) and Johnson et al. (2004) were pioneers in using aerial remote sensing for monitoring the coffee ripeness. By using UAV images, these authors found that the spectral response of the crop canopy was highly correlated ($r = 0.81$) with the fruit ripeness, especially in fields with high fruit display on the canopy. However, despite finding promising results, these studies were conducted at the field level, which does not consider the spatial variability of the fruit ripeness. Since arabica coffee blossoms do not appear and develop uniformly throughout the field, the spatial and temporal

* Corresponding author at: Instituto Federal do Norte de Minas Gerais (IFNMG), Araçuaí, Brazil.

E-mail address: rodrigo.nogueira@ifnmg.edu.br (R. Nogueira Martins).

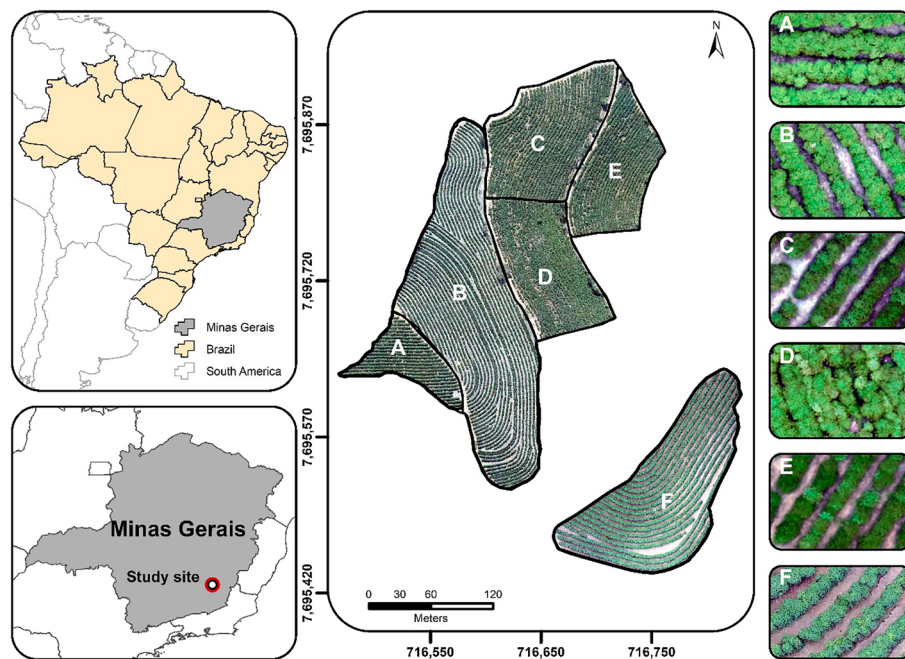


Fig. 1. Location of the study site in the *Zona da Mata* region of Minas Gerais State, Southeastern Brazil. The rectangular boxes on the right side of the figure present an aerial view of each coffee field.

variability of fruit ripeness among trees as well as within a single tree is practically inevitable (DaMatta et al., 2007).

To overcome the limitation of not analyzing the spatial variability of fruit ripeness, Rosas et al. (2021) used different VIs derived from a low-cost multispectral camera onboard a UAV for monitoring the fruit ripeness at the plant level. Results showed that the VIs were able to discriminate plants with unripe fruits from those with ripe fruits in most fields. However, their performance was mostly affected by the canopy volume and crop yield. Similarly, Nogueira Martins et al. (2021) used spectral information obtained from different cameras and developed a novel VI for monitoring the fruit ripeness. The coffee ripeness index (CRI) was validated under different analysis and presented superior performance over different VIs. However, there is still a gap in the

literature to develop strategies for mapping the fruit ripeness spatial variability remotely, as well as to aid in the definition of the ideal harvest time.

Recent published works have concentrated only on the spectral information of UAV imagery, but the spatial information in the form of texture remains unexplored. Spectral variables represent the average tonal variations in various bands, whereas textural variables contain information about the spatial distribution of tonal variations of pixels within a defined area of an image (Haralick et al., 1973; Wang et al., 2021). In contrast, the use of textural variables derived from UAV images can enhance the detection of finer vegetation structural features (Schumacher et al., 2016). Therefore, the use of textural variables has potential for improving the fruit ripeness prediction and mapping.

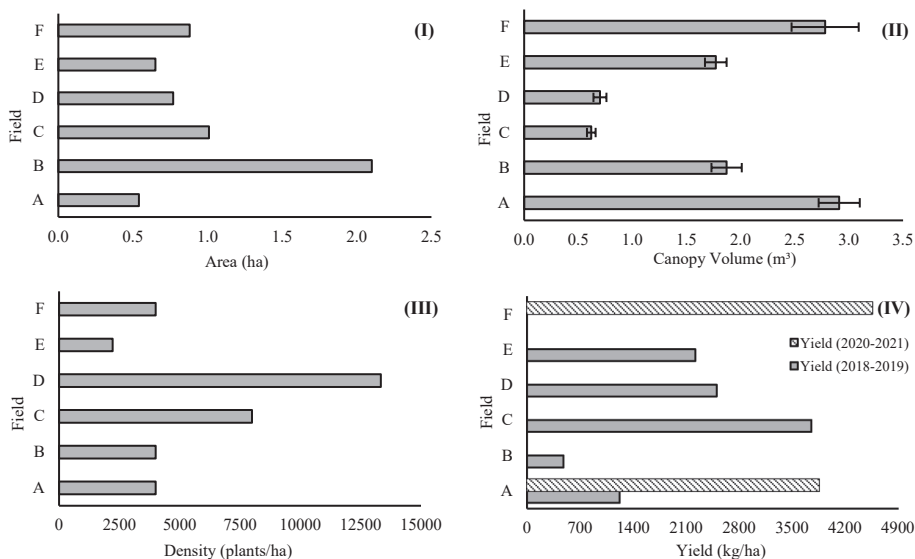


Fig. 2. Cultivation area (I), canopy volume (II), density of plants (III), and yield (IV) of the coffee fields evaluated in this study. For fields A, B, D, and E the coffee fruits were red when ripe; conversely, in field C they were yellow when ripe. The crop yield refers to the 2018–2019 (Fields A, B, C, D, and E), and 2020–2021 seasons (Fields A and F).

Table 1

Unmanned Aerial Vehicles (UAV) imagery collection timeline and flight parameters.

Season	Field	Date	Overlap (%) ¹	AGL (m) ²	GSD (m) ³
2018–2019	A, B, C, D, and E	13/05/2019			
	A, B, C, D, and E	27/05/2019			
	A	04/05/2021			
	F	10/05/2021	80 / 75	60	0.05
2020–2021	A	18/05/2021			
	A and F	24/05/2021			
	F	31/05/2021			

¹ Lateral and longitudinal overlap; ²AGL, Above ground level; and ³GSD, Ground sampling distance.

Previous research works that compared the use of either spectral or textural variables alone to the combination of both variables have shown that the latter resulted in better performance for crop yield prediction (Wang et al., 2021), nitrogen status estimation (Fu et al., 2020), and crop biomass and leaf area index predictions (Dos Reis et al., 2020; Fu et al., 2021). Thus, since UAV images present spatial resolution at centimeter-level and comprise rich spatial information of observed objects, the use of spectral information combined with textural information for improving fruit ripeness prediction and mapping becomes possible.

Based on that, it has been hypothesized that the use of spectral bands and VIs combined with textural variables derived from UAV imagery could potentially improve the performance of prediction models for coffee fruit ripeness mapping. Therefore, the objectives of this study were to: (1) predict the fruit ripeness using spectral and textural variables; and (2) to determine the best variables for developing spatio-temporal variability maps of the fruit ripeness.

2. Material and methods

2.1. Study site

The study site ($42^{\circ}55'11.906''$ W; $20^{\circ}49'26.158''$ S and $42^{\circ}55'1.076''$ W; $20^{\circ}49'39.997''$ S) is located in the municipality of Paula Cândido, Minas Gerais State, Brazil (Fig. 1). According to the Köppen-Geiger Climate Classification, the climate of the region is Cwa (humid subtropical), with a rainy season in the summer and dry winter (Alvares et al., 2013).

This study was conducted in six fields of arabica coffee (*Coffea arabica* L.) with a total area of 5.95 ha. These fields were represented by the following cultivars: Red Catuai (Fields A, B, and F), MGH 4191 (Field C), Red Bourbon (Field D), and Icatu (Field E). In addition, all fields presented distinct characteristics for the cropped area, fruit color, canopy volume, plant density, and yield (Fig. 2).

2.2. UAV imagery acquisition and processing

Imagery acquisition in the study site was performed using a quadcopter (model: Matrice 100, DJI Innovations, Shenzhen, China) equipped with a multispectral camera (model: RedEdge MX, MicaSense, Seattle, USA). The RedEdge MX contains five CMOS (complementary metal oxide semiconductor) sensors, which captures five spectral bands in the following wavelengths: (1) Blue (455–495 nm); (2) Green (540–580 nm); (3) Red (658–678 nm); (4) Rededge (RE) (707–727 nm); and (5) Near-infrared (NIR) (800–880 nm) (DadrasJavan et al., 2019).

Table 2

Summary of the vegetation indices used in this study.

Vegetation Index	Equation	Reference
CRI	$(R/R_{target}) \times 100$	(Nogueira Martins et al., 2021)
GRRI	(G/R)	(Johnson et al., 2004)
MCARI1	$1.2[2.5(NIR - R) - 1.3(NIR - G)]$	(Haboudane et al., 2004)
PSRI	$(R - B)/N$	(Merzlyak et al., 1999)
NDRE	$(N - RE)/(N + RE)$	(Fitzgerald et al., 2006)
NGRDI	$(G - R)/(G + R)$	(Zheng et al., 2018)
EXR	$1.4R - G$	(Meyer and Hindman, 1998)

R, Red; G, Green; B, Blue; RE, Rededge; N, Near-infrared; and R_{Target} , Average reflectance value of the red target in the red band.

Table 3

Summary of the texture variables used in this study.

Textural Variables	Equation	Meaning
Mean (MEA)	$\sum_{i,j=0}^{N-1} P_{ij}$	Gray level average in the GLCM window.
Variance (VAR)	$\sum_{i,j=0}^{N-1} i P_{ij} (i - MEA)^2$	Gray level variance in the GLCM window.
Homogeneity (HOM)	$\sum_{i,j=0}^{N-1} i (P_{i,j}) / (1 + (i - j))^2$	A measure of homogenous pixel values across an image.
Dissimilarity (DIS)	$\sum_{i,j=0}^{N-1} i P_{ij} i - j $	Similar to contrast and inversely related to homogeneity.
Contrast (CON)	$\sum_{i,j=0}^{N-1} i P_{ij} (i - j)^2$	Measures the local variations among neighboring pixels in the GLCM matrix.
Entropy (ENT)	$\sum_{i,j=0}^{N-1} i P_{ij} (-\ln P_{ij})$	Represents the degree of disorder present in the image. The value of entropy is the largest when all elements of the cooccurrence matrix are the same and small when elements are unequal.
Second moment (SM)	$\sum_{i,j=0}^{N-1} i (P_{i,j})^2$	A measure of homogeneity of the image.
Correlation (COR)	$\sum_{i,j=0}^{N-1} i P_{ij} \left[\frac{(i - MEA)(j - MEA)}{\sqrt{VAR_i VAR_j}} \right]$	Measures the joint probability occurrence of the specified pixel pairs.
Notes:	$P_{ij} = V_{ij} / \sum_{i,j=0}^{N-1} V_{ij}$	GLCM is the grey level co-occurrence matrix; V_{ij} is the value in the cell i, j (row i and column j) of the moving window; and N , is the number of rows or columns. Adapted from Haralick et al. (1973), and Wang et al. (2021).

The UAV flights were conducted between 11:00 and 13:00 h local time under clear-sky conditions on seven dates within the 2018–2019 and 2020–2021 seasons (Table 1). For that, a flight plan previously defined in the DroneDeploy software (DroneDeploy Inc., San Francisco, CA, USA) was used. All flights were carried out at 9.3 m s^{-1} speed at 60 m above ground level with 80% front overlap and 75% side overlap between images. In addition, before and after each flight, images of the reflectance calibration target provided by the manufacturer were taken at 1.00 m height to perform the radiometric calibration in postprocessing.

After the flights, all images were stored in RAW format and after processing converted to the Tagged Image File Format (TIFF). All images were processed using the Agisoft™ MetaShape software, version 1.5.3 (Agisoft LLC, St. Petersburg, Russia) following the same procedures from the image alignment to the creation, and georeferencing of the orthomosaics as detailed in Nogueira Martins et al. (2021). The

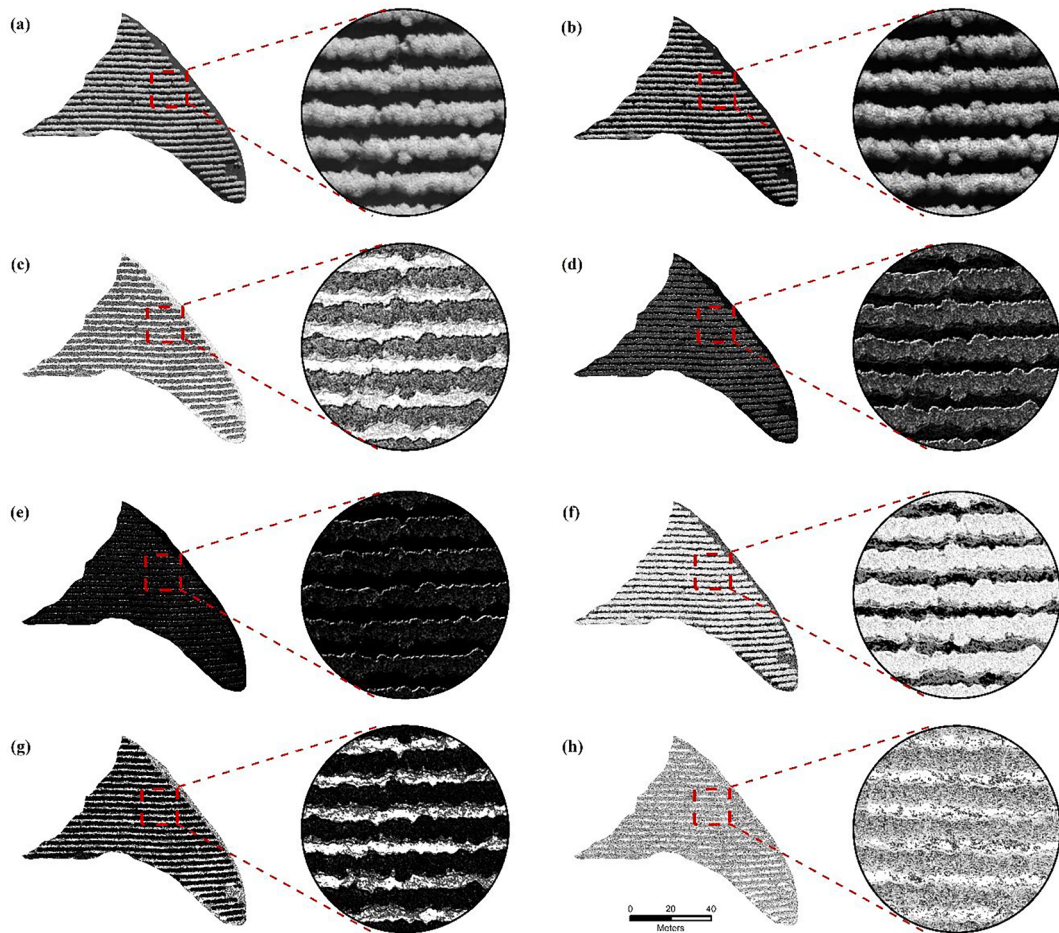


Fig. 3. GLCM-based texture variables: mean (a), variance (b), homogeneity (c), dissimilarity (d), contrast (e), entropy (f), second moment (g), and correlation (h) obtained from the NIR band in 04/05/2021.

georeferencing of the orthomosaics was conducted in the QGIS software, version 3.2 (QGIS Development Team, 2016) using the information from 20 ground control points (GCP), which were placed on the area before the flights. These GCPs were georeferenced using a topographic GNSS (Global Navigation Satellite System) receiver, model Trimble ProXT (Trimble Inc., Sunnyvale, CA, USA).

2.3. Spectral and textural data extraction

In this study, the spectral bands Red, Green, Blue, RE, and NIR and the following VIs: Coffee Ripeness Index (CRI); Green-red Ratio Ripeness Index (GRRI); Modified Chlorophyll Absorption in Reflectance Index 1 (MCARI1); Plant Senescence Reflectance Index (PSRI); Normalized Difference RedEdge Index (NDRE); Normalized Green-red Difference Index (NGRDI); and Excess of Red (EXR) were obtained from the UAV images (Table 2). These VIs were chosen based on their sensitivity to changes in the canopy structure and fruit ripeness as well as to changes in pigment and plant nutritional status.

In addition to the spectral bands and VIs, the grey level co-occurrence matrix (GLCM) was used to compute textural variables. The GLCM is a matrix where the number of rows and columns is equal to the number of gray levels in the image. Basically, the GLCM interprets the spatial distribution of pairs of pixel separated by a certain distance in a given direction (Liu et al., 2019). Eight textural variables proposed by Haralick et al. (1973), including mean (MEA), variance (VAR), homogeneity (HOM), dissimilarity (DIS), contrast (CON), entropy (ENT), second moment (SM), and correlation (COR) were obtained in this study (Table 3). The texture variables were obtained using the smallest

Table 4
Summary of the textural indices used in this study.

Vegetation Index	Reflectance-based Equation	Texture-based Equation
NDTI	–	$(T_\lambda - T_i)/(T_\lambda + T_i)$
NDVI	$(R_N - R_R)/(R_N + R_R)$	$(T_N - T_R)/(T_N + T_R)$
GNDVI	$(R_N - R_G)/(R_N + R_G)$	$(T_N - T_G)/(T_N + T_G)$
NDRE	$(R_N - R_{RE})/(R_N + R_{RE})$	$(T_N - T_{RE})/(T_N + T_{RE})$

moving window size (3×3 pixels) with an orientation of 45° (1,1) due to the UAV imagery spatial resolution (0.05 m), and to the absence of significant heterogeneity between other orientations (Fu et al., 2021).

The textural analysis resulted in eight variables for each spectral band (RGB, RE, and NIR) (Fig. 3). These variables were named using the first letter of the band's name in combination with the texture metric's name (e.g., Rmean, Bmean, Gmean, Nmean, and REmean). This process was performed for all texture metrics. Further, a detailed description of the eight texture measurements used in this study is presented elsewhere (Soares et al., 1997). All textural variables were obtained using the R software, version 3.5.1 through the GLCM package (R Core Team, 2021; Zvoleff, 2020).

Since textural variables are single band parameters, they can be used to develop textural indexes. Thus, textural variables from different bands can formulate different indexes such as the spectral VIs used in this study. In this sense, the VIs NDVI (Normalized Difference Vegetation Index), GNDVI (Green Normalized Difference vegetation Index), and NDRE were used as a reference for calculating a normalized difference texture index (NDTI) (Gitelson et al., 1996; Rouse et al., 1973; Zheng

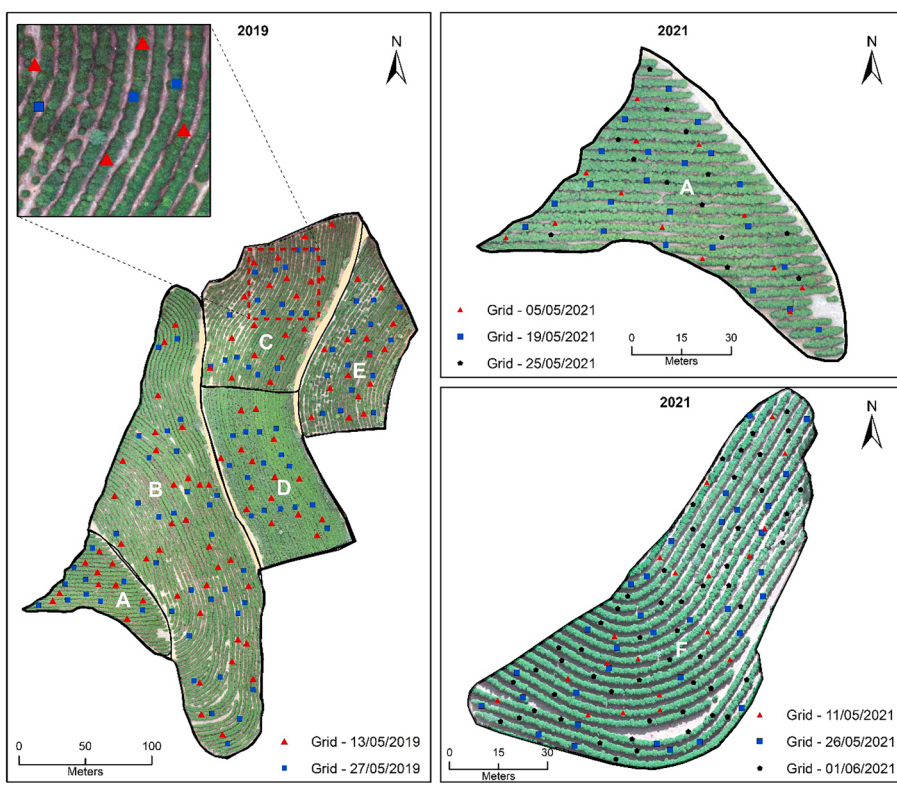


Fig. 4. Spatial distribution of the sampling points used for field measurements of the coffee ripeness.

et al., 2019). The NDTI was obtained using the two-band combinations from all textural variables (mean, variance, homogeneity, dissimilarity, contrast, entropy, second moment, and correlation) (Table 4). Then, all the NDTI-based VIs were named from NDTI1 to NDTI8 according to the eight texture metrics. This process was repeated to the NDVI, GNDVI, and NDRE indices.

R_R , R_G , R_N , and R_{RE} refer to the reflectance of the red, green, near-infrared, and reededge bands, respectively; and T_R , T_G , T_N , and T_{RE} refer to the texture variables derived from the red, green, near-infrared, and reededge spectral bands, respectively.

Finally, from the coordinates of the sampling grid, polygonal masks (region of interest) for each sampling point were created in the QGIS software. The polygons covered three plants in a row that were used to represent each point. Then, the average values of the 76 predictor variables (5 spectral bands, 7 vegetation indices, 40 texture bands, and 24 texture indices) within the polygons were extracted using the zonal statistics tool. The dataset obtained from the images was arranged in an X matrix (predictors) and the fruit ripeness (percentage of unripe fruits) measured on the field was arranged in the Y vector (response variable).

2.4. Field data collection

Coffee fruit ripeness was measured on seven dates during the 2018–2019 crop season (May 13th and May 27th, 2019) for fields A, B, C, D, and E and in the 2020–2021 season for fields A (May 05th, 19th, and 25th, 2021), and F (May 19th and 25th and June 01st, 2021). For that, an irregular sampling grid with 20 sampling points per hectare was defined on each date for fields A, C, D, E, and F (Fig. 4). For field B, only 10 points per hectare were collected due to its lower fruit load. The sampling points were represented by three plants located side by side in the same cultivation row. Then, four plagiotropic branches, one per plant quadrant were randomly chosen in the middle third of each plant. Finally, the average value of unripe fruits and the total of fruits were determined and used to represent each sampling point. From now on, the percentage of unripe fruits will be referred to as fruit ripeness.

2.5. Data modeling

To develop and validate the predictive models, the two-year experimental data were randomly split into training ($n = 227$, 70%) and testing ($n = 96$, 30%) datasets. The training dataset was used for pre-processing of data, selection of optimal variables, and optimization of hyperparameters, while the testing dataset was used with the final model to predict the fruit ripeness. The predictive models were developed using six machine learning (ML) methods, including the random forest (RF), support vector machine with linear kernel (SVM), gradient boosting machine (GBM), bagged cart (BC), bayesian ridge regression (BRR), and the artificial neural networks (ANN). These methods were implemented through the R software using the packages ‘randomforest’, ‘e1071’, ‘nnet’, and ‘caret’ (Breiman, 2001; Kuhn, 2008; Meyer et al., 2019; Venables and Ripley, 2002).

Furthermore, to evaluate the potential influence of the texture variables to predict the fruit ripeness, two scenarios including as predictors only the spectral variables (bands and VIs) (1); and the combination of spectral and textural variables (2) were evaluated. Prior to training the ML models, the recursive feature elimination (RFE) method was used for variable selection, removing the variables of minor importance based on the performance of the k-fold cross-validation (5 folds) with 10 repeated experiments. Then, a Pearson correlation analysis was carried out to assess the association of the selected variables with the fruit ripeness.

Next, the hyperparameters from all ML models were fine-tuned using the grid search method and selected according to the accuracy estimation in the training dataset. These analyses were performed using the ‘caret’ package. In addition, to analyze the relative importance of the predictors in the ML models, the built-in function ‘varImp’ from the ‘caret’ package was used to rank the variable importance for each prediction model. The performance of the ML models was evaluated using the coefficient of determination (R^2), and the root-mean-square error (RMSE) for the testing dataset. All modeling analyses and evaluations were performed using R the software. The flow chart of data processing and statistical analyses for prediction and mapping the fruit ripeness is

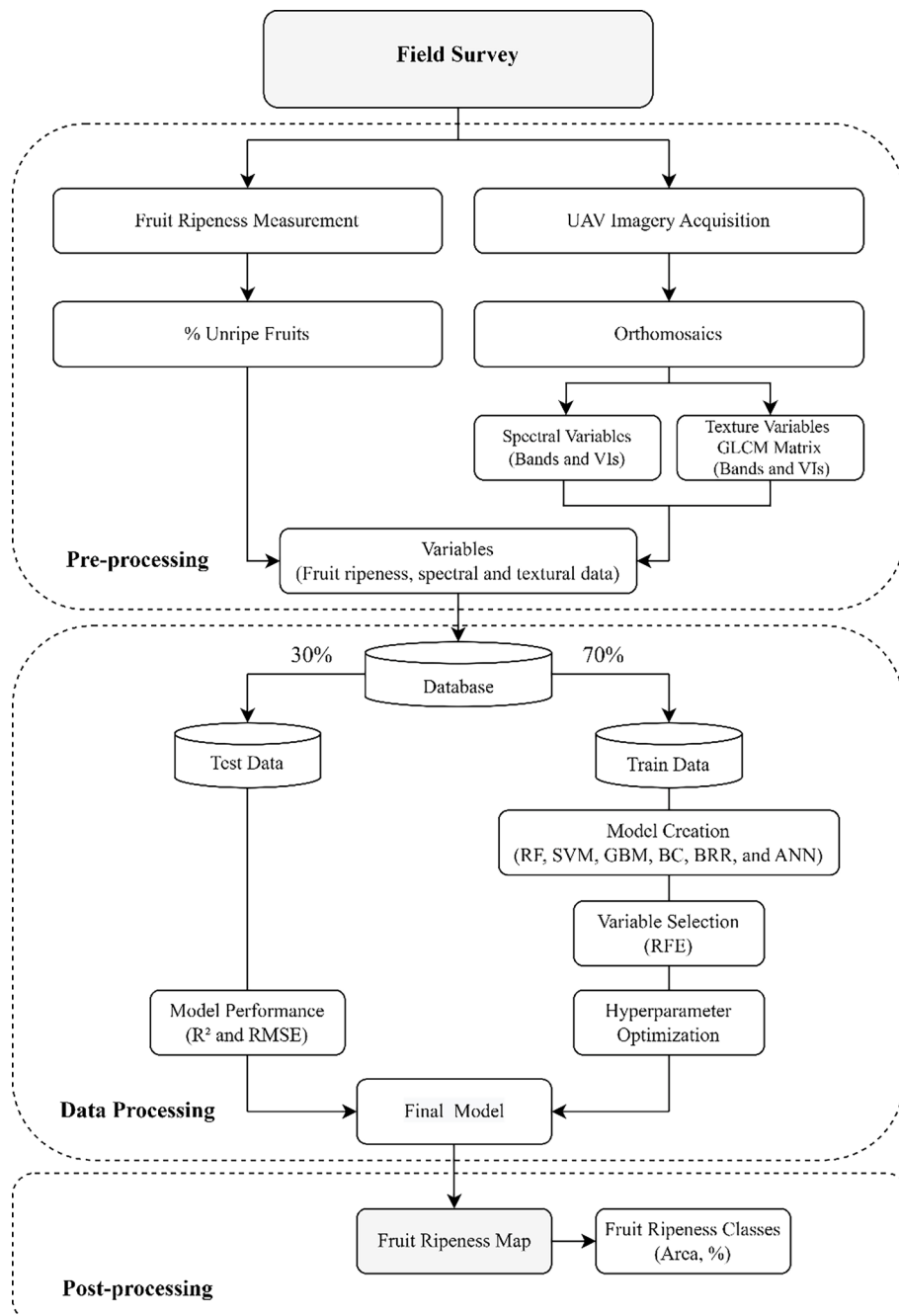


Fig. 5. Flowchart of the fruit ripeness prediction and mapping.

presented in Fig. 5.

After testing the ML models, the whole imagery dataset, including the spectral and textural variables, was used as input for mapping the spatial distribution of the fruit ripeness. This process was performed using the ‘raster’ package (Hijmans et al., 2012) by combining the predictor variables (raster) into a single multi-layered (.tif) file, which was then used as input to predict each pixel through the ML model that presented the best performance among all six models. Then, the fruit ripeness maps were arranged in a layout with different classes, whose area (m^2 and %) were later obtained to assess the temporal evolution of the fruit ripeness.

3. Results

3.1. Relationships between spectral and texture variables and the fruit ripeness

Among the 76 variables (12 spectral and 64 textural variables) created for developing the prediction models, the variable selection using the RFE method resulted in 10 and 19 variables, respectively for scenarios 1 and 2. Then, a Pearson correlation analysis between the selected variables with the fruit ripeness was performed. Significant correlations ($p < 0.05$) were found between the majority of the selected variables (Fig. 6). Overall, the highest correlation (r) values were presented by the spectral variables, which ranged from -0.7 (CRI) to 0.2 (EXR). Conversely, for the textural variables, when significant, the r values varied from -0.22 (Nvariance) to -0.12 (NDVI1).

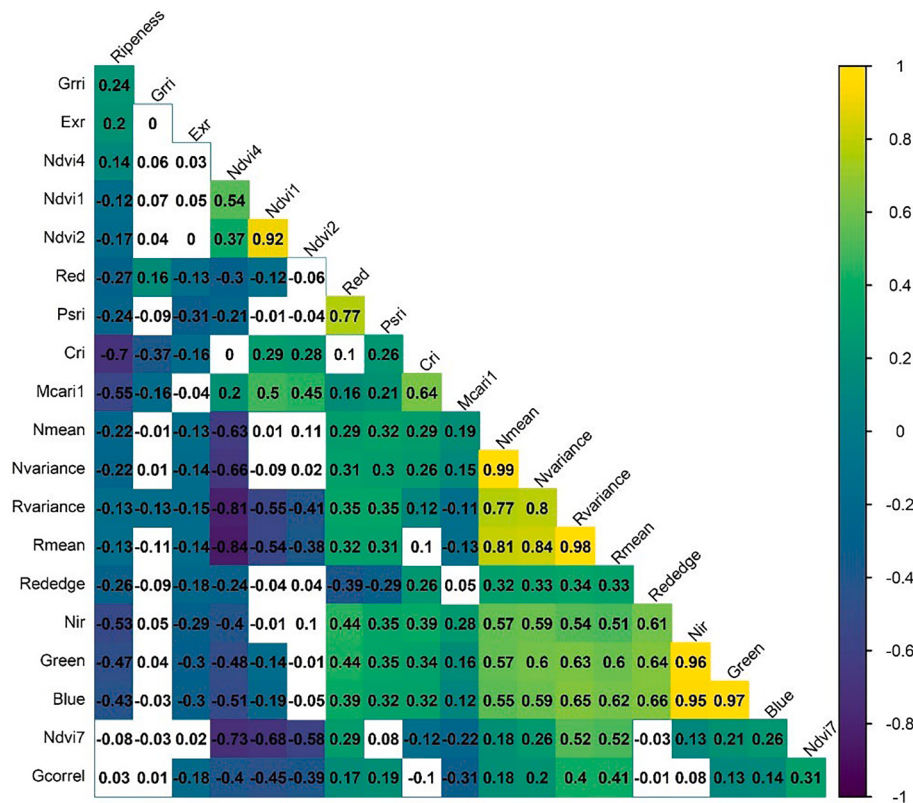


Fig. 6. Pearson's correlation matrix between the fruit ripeness and the selected spectral and textural variables. Colored correlations are significant by test t ($p < 0.05$).

3.2. Prediction of fruit ripeness with spectral and textural variables

The ML models based solely on the selected spectral variables (spectral bands and VIs) demonstrated moderated accuracy in the fruit ripeness prediction; however, lower than the second scenario, whose ML models used as predictors, the combination of spectral and textural variables (Fig. 7). Together these variables improved the accuracy of the ML algorithms, whose increase in the R^2 values for the test dataset ranged from 5.97 to 6.55%, while the decrease in the RMSE values ranged from 5.86 to 5.62% between both scenarios in the six ML algorithms.

Among the selected variables that were used as predictors, the spectral bands and VIs presented the highest importance (%) in the construction of the ML models. For both scenarios, the variables CRI, Red, MCARI, and NIR were the ones that contributed most to the fruit ripeness prediction (Fig. 8). The total importance of these variables ranged from 48.56 to 61.01% and from 39.17 to 59.62% in scenarios 1 and 2, respectively. On the other hand, despite increasing the performance of the majority of the ML models, except for the BC and ANN models, when combined with the spectral variables, the textural variables showed a small contribution to the prediction models. Among the textural variables, the NDVI1, NDVI4, and NDVI7 were the ones that presented the highest importance in most of the ML models. The remaining variables contributed similarly to other spectral variables whose importance ranged from 0.60 to 4.05%.

3.3. Spatiotemporal variability maps of the fruit ripeness

The spatiotemporal variations in the fruit ripeness are shown in the maps obtained with the RF-based models, which presented best performance among the evaluated ML algorithms. Due to the higher availability of imagery, only the maps of fields A and F are presented (Figs. 9 and 10). Predicted fruit ripeness (% unripe fruits) ranged from

17.65 to 85.34% within the sampling dates of both coffee fields. In addition, as observed in the field, the maps also presented a high spatial and temporal variability of fruit ripeness among trees as well as within a single tree. The spatiotemporal evolution of the fruit ripeness throughout the field samplings is highlighted on the maps through the dashed rectangles, which presents an amplified view of the crop rows. Regarding the visual difference in the maps from both scenarios, the maps obtained with spectral and textural variables, especially for field A, provided a better visual of the spatiotemporal variations in the fruit ripeness degree.

Overall, the spatiotemporal changes agreed with the expected reduction of the percentage of unripe fruits over time, as driven by the temporal evolution of the fruit ripeness. For field A, when looking at the fruit ripeness classes, the area of plants within the two first classes (17.65 – 48.18% of unripe fruits) increased from 44.66 to 55.29% and from 46.04 to 58.03% from May 04th to May 24th, 2021, respectively, for scenarios 1 and 2. Conversely, the area of plants with a higher percentage of unripe fruits decreased from 55.34 to 44.71% and from 53.96 to 41.97% respectively, for scenarios 1 and 2 (Table 5). In this field, major changes were observed between the two first sampling dates due to the higher interval of days.

Similarly, the temporal changes in the percentage of unripe fruits in the field F were detected on the maps as the fruit ripeness progressed (Fig. 10 and Table 6). In this field, the area of plants included in the two first classes increased from 60.04 to 88.91% and from 54.2 to 87.87% from May 10th to May 31st, 2021, respectively, for scenarios 1 and 2. When compared to field A, it can be noted that field F presented a more accentuated change between the fruit ripeness classes.

When looking at the maps, specifically for field A, it can be seen that the upper side of the plants presented a lower percentage of unripe fruits when compared to the lower side (Fig. 9). This situation occurred due to the planting orientation of the coffee rows (from west to east), whose plant's upper side receives a higher incidence of solar radiation

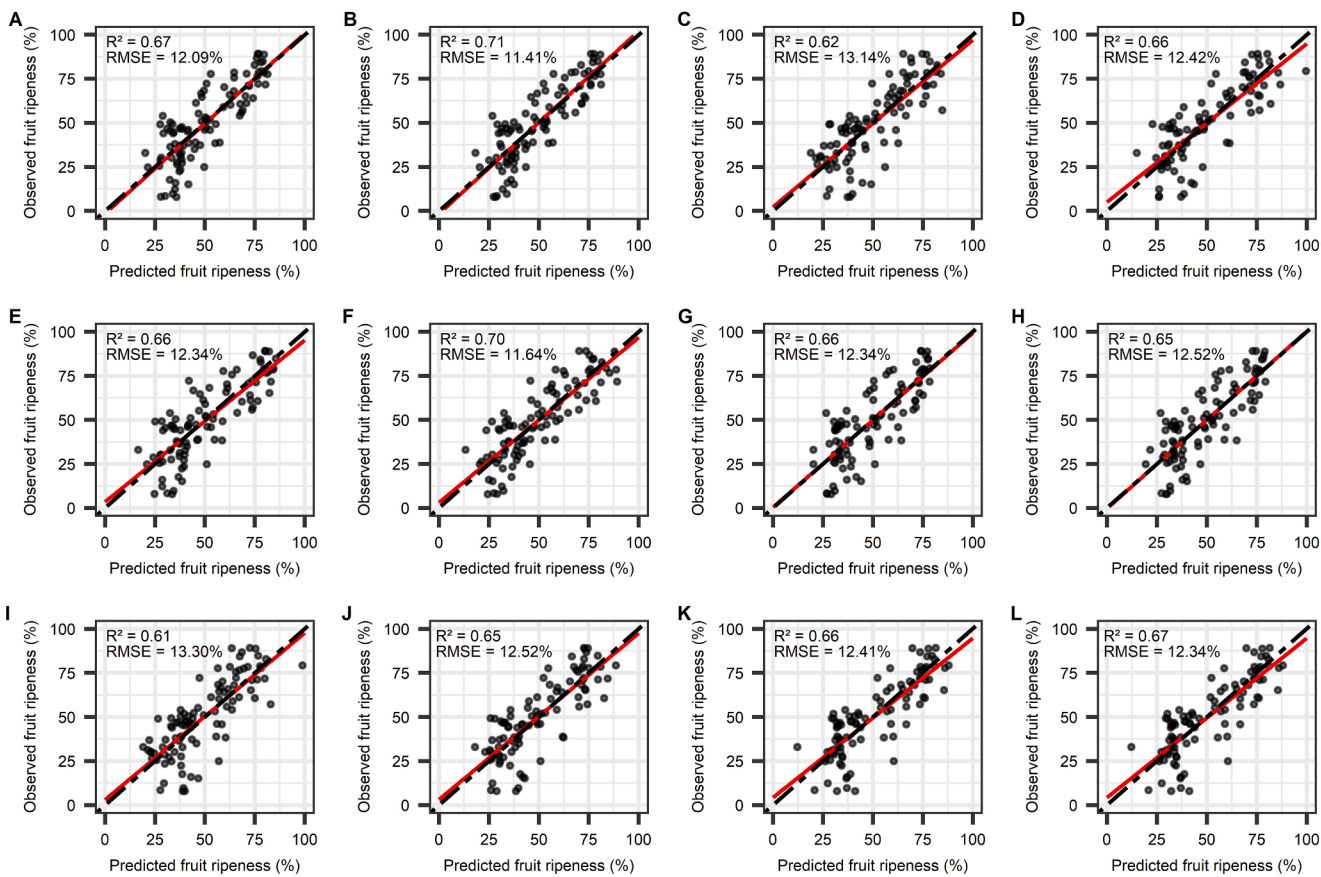


Fig. 7. Scatterplots of the predicted versus observed values of fruit ripeness obtained using as input only the spectral variables, and the combination of spectral and textural variables for the random forest (A and B), support vector machine with linear kernel (C and D), gradient boosting machine (E and F), bagged cart (G and H), bayesian ridge regression (I and J), and artificial neural network (K and L) machine learning methods.

throughout the day. These differences in the fruit ripeness degree were also observed during the field campaigns.

Moreover, for both fields, the presence of shadows during the image acquisition ended up influencing the prediction and the spatial variability of the fruit ripeness in some maps. For field A, a higher percentage of unripe fruits can be observed on the left end of the field on May 18th, 2021 (Fig. 9B and 9E). Differently, in field F these errors were mostly present throughout the left side of the field on May 31st, 2021 (Fig. 10C and 10F). Despite the efforts, the presence of shadows on the imagery was unavoidable on some days since the coffee fields were surrounded by a eucalyptus plantation. Regardless, the spatiotemporal variability maps enabled the detection and quantification of the fruit ripeness changes over time, showing that this methodology can be used to replace the time-consuming fieldwork.

4. Discussion

In recent years, the use of multispectral cameras mounted on unmanned aerial vehicles (UAVs) has shown to be a feasible way for crop monitoring using remotely sensed data (Rosas et al., 2020). Based on that, this study addressed the feasibility of using spectral and textural variables derived from UAV imagery to predict and map the spatio-temporal variability of the fruit ripeness in six coffee fields with distinct characteristics.

4.1. Spectral and textural data fusion and its impact on model accuracy

Previous studies focused on monitoring the coffee ripeness used only spectral variables (bands and VIs) leaving the inherent spatial information in the form of texture unexplored (Herwitz et al., 2004; Johnson

et al., 2004; Nogueira Martins et al., 2021; Rosas et al., 2021). Textural variables derived from high-resolution imagery enable a much better discrimination of vegetation structure (Dos Reis et al., 2020). Recent studies have shown that textural variables, not only increased the data dimensionality of UAV imagery with countable bands and VIs but improved the accuracy of prediction models for several crop parameters when combined with spectral data (Liu et al., 2019; Zheng et al., 2019). Accordingly, this study demonstrated that compared to the ML models based solely on spectral variables, the incorporation of textural variables increased the accuracy of the fruit ripeness prediction by reducing the RMSE from 13.30 to 11.41% and increasing the R^2 from 0.61 to 0.71 (Fig. 7). This indicates, to some extent, that textural variables aggregate valuable information for remote monitoring of the coffee crop.

Even though the prediction models that used spectral and textural variables presented superior accuracy, except for the bagged cart and artificial neural networks models, when looking at the variable importance metric of the six ML algorithms, the most important texture variable ranked only as top-5 in the best situation (NDVI1 in the RF model; Fig. 8B and NDVI1 in the ANN model; Fig. 8L), whereas the spectral variables CRI, Red, MCARI1, and NIR presented the greatest contribution for the majority of the ML models (Fig. 8). This result can be explained by the way the spectral and textural values were obtained, and to what they represent.

While spectral variables detect the tonal variations at the pixel level, textural variables measure the heterogeneity in the tonal values of pixels within a defined area of an image (Wood et al., 2012). Thus, since the textural variables were obtained using a GLCM window (3×3 pixels), the pixel values that contained information from leaves and fruits (crop canopy) were smoothed, which ended up reducing the sensitivity of these variables to detect the temporal changes of the fruit color.

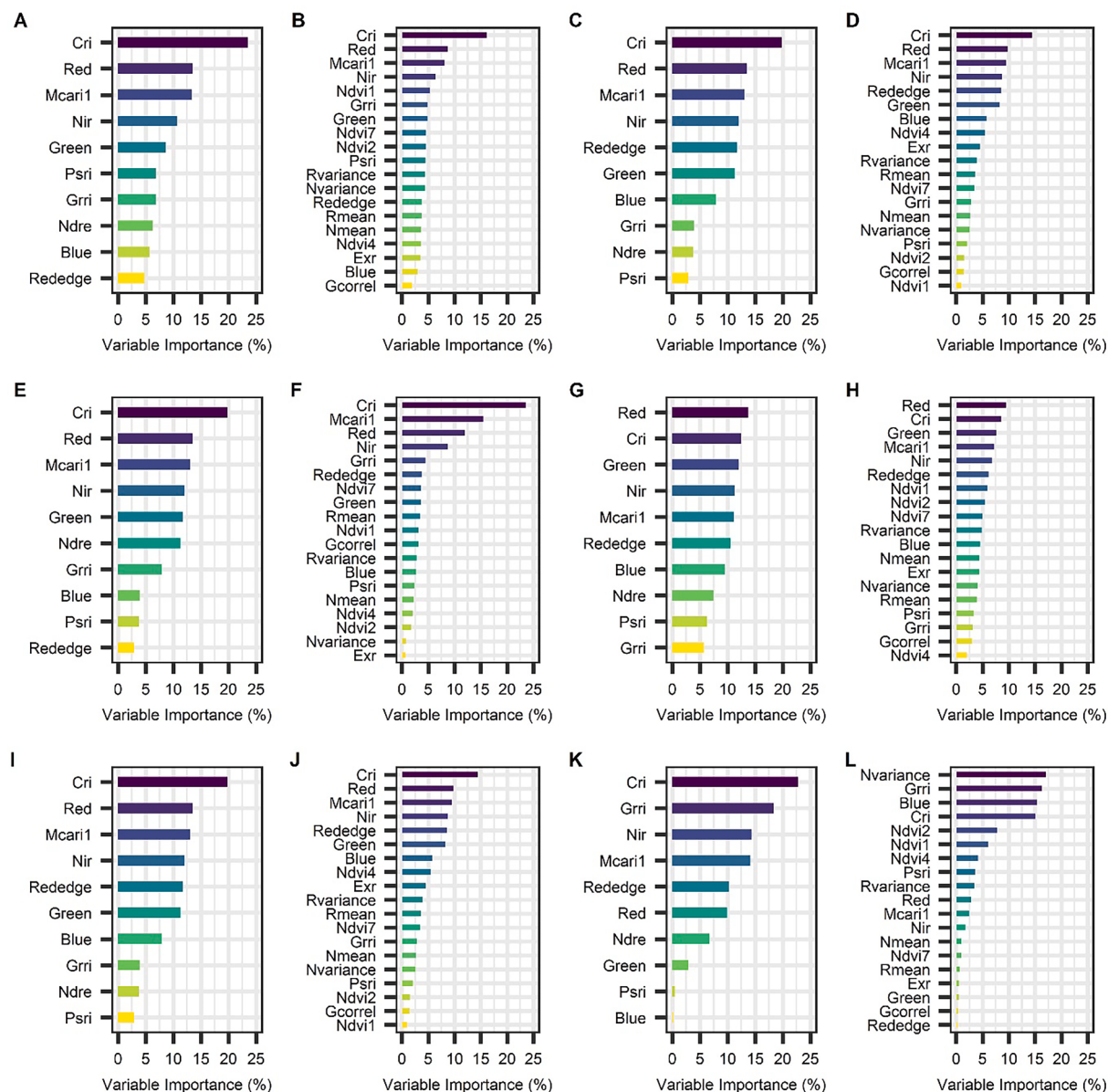


Fig. 8. Variable importance attributed by the random forest (A and B), support vector machine with linear kernel (C and D), gradient boosting machine (E and F), bagged cart (G and H), bayesian ridge regression (I and J), and artificial neural network (K and L) machine learning methods for prediction of the fruit ripeness using only the spectral variables and the combination of spectral and textural variables.

Conversely, the spectral variables presented higher sensitivity to detect the changes on the crop canopy as they were extracted at the pixel level. Finally, the greater importance of the spectral variables is supported by the correlation analysis, in which these variables presented a higher association with the fruit ripeness than the textural variables (Fig. 6).

When compared to previous studies, all ML models when using as input the spectral variables outperformed the linear regression approach used by Nogueira Martins et al. (2021). These authors used different VIs in five coffee fields and obtained an R^2 of 0.57 and RMSE of 14.60% when all fields were evaluated together. On the other hand, Herwitz et al. (2004) reported a higher correlation (R^2 : 0.81; RMSE not available) in seven coffee fields. However, this analysis was carried at field level, which does not fully represent the spatiotemporal variability of the fruit ripeness. Therefore, these results highlights the suitability of the ML algorithms, especially the RF that presented the best performance, to be used as a baseline for the development of prediction models using UAV-derived data. Furthermore, this study filled a gap in the literature by developing the fruit ripeness spatial variability maps,

which can be used as decision support tools for monitoring and identifying on a temporal scale the area of plants ready and not ready for harvest throughout the end of the season.

4.2. Factors influencing the remote monitoring of coffee fruit ripeness

The factors influencing the remote monitoring of the coffee crop are mainly related to the crop spectral response, which in turn is influenced by the crop characteristics (e.g., canopy architecture and size, plant density, and yield), agrometeorological conditions, and the presence of biotic and abiotic stresses (Bernardes et al., 2012; Johnson et al., 2004; Louzada Pereira et al., 2018; Marin et al., 2021; Nogueira Martins et al., 2021; Rosas et al., 2021). Regarding the fruit ripeness monitoring, the most limiting factors were the plant density, canopy volume, and crop yield as reported in previous studies.

Studies conducted by Johnson et al. (2004) and Herwitz et al. (2004) showed that the fruit ripeness was related to the spectral variables, but only in certain fields with significant fruit display on the crop canopy.

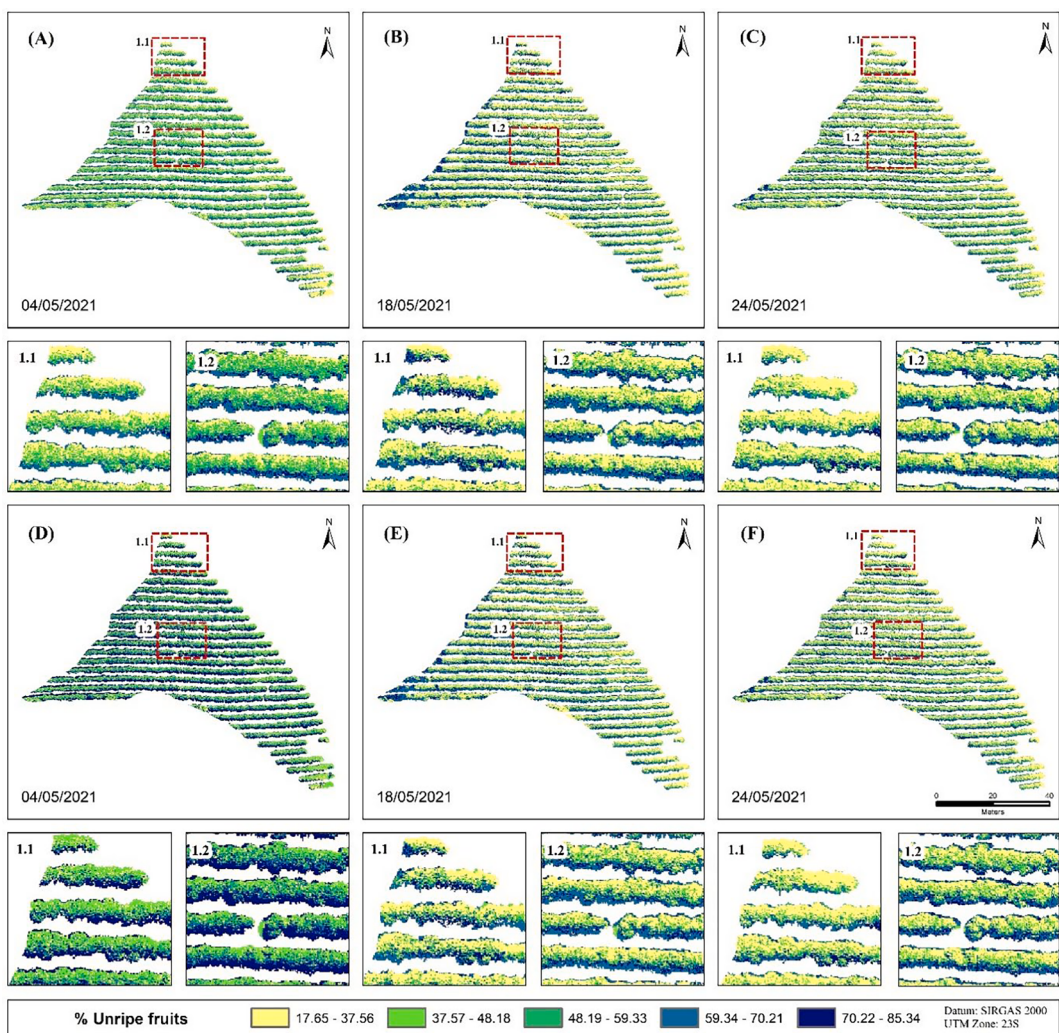


Fig. 9. Spatial variability maps of the fruit ripeness (% unripe fruits) obtained with the random forest models using as predictors the spectral variables (A, B, and C) and the combination of spectral and textural variables (D, E, and F) from field A in 2021. The dashed rectangles identified as 1.1 and 1.2 on the maps represent an amplified view of the crop rows.

More recently, Rosas et al. (2021) and Nogueira Martins et al. (2021) used different VIs for monitoring the fruit ripeness at the plant level in coffee fields with distinct characteristics of canopy volume, crop yield, cultivar, and plant density. The results showed that the interaction between crop yield and canopy volume were the main factors affecting the performance of the VIs. The combination of high crop yields with low canopy volumes resulted in a greater amount of exposed coffee fruits, which caused a greater spectral change on the crop canopy and that were detected by the spectral variables during the ripening stage.

In this study, although the spectral and textural information from all fields were used together to build a global model, differences in the spatiotemporal variability maps from fields A and F were found when the fruit ripeness classes were discriminated. The field F presented a more accentuated change between the fruit ripeness classes when compared to field A. These differences are possibly associated with the lower crop canopy (Fields A and F: 2.91 and 2.78 m³) and the higher yield on this field (Fields A and F: 3850 and 4550 kg ha⁻¹) (Fig. 2).

In addition, another factor that influenced the fruit ripeness spatial variability was the unequal fruit ripening in different sides of the plants. Specifically for field A, it was observed during the field campaigns and, also, through the maps that the upper side of the plants presented a lower percentage of unripe fruits when compared to the lower side (Fig. 9). This difference is possibly related to the planting orientation of the coffee rows (from west to east), in which the upper side of the plants

are submitted to a higher incidence of solar radiation throughout the day. According to Cannell (1975), the initiation of the flower buds requires higher light intensities. In this sense, due to its greater insolation, the upper side of the plant may be receiving the “start” of the floral induction before the lower side, with an additional flowering beforehand. This may explain the occurrence of a higher percentage of ripe fruits on the upper side of the plants. The influence of solar radiation on coffee ripeness, and especially on the beverage quality has been discussed elsewhere (Louzada Pereira et al., 2018). Lastly, the visual quality of the image is also a limiting factor, especially when there is the presence of shadows and/or blur that can alter the reflectance values in the image. Here, the presence of shadows, which was unavoidable on some dates, ended up influencing the spatial variability of the fruit ripeness in specific areas of the maps.

4.3. Limitations and directions for future studies

The main limitations of this study are related to the crop characteristics, unequal fruit ripening, and image quality as discussed before. Since the coffee crop presents a complex spectral behavior that is highly influenced by the dense plant canopy, which in turn is composed of a mixture of green leaves, unripe, ripe, and overripe fruits; thus, spectral confusion and errors of underestimation or overestimation in the prediction models are unavoidable. In general, the aerial monitoring of the

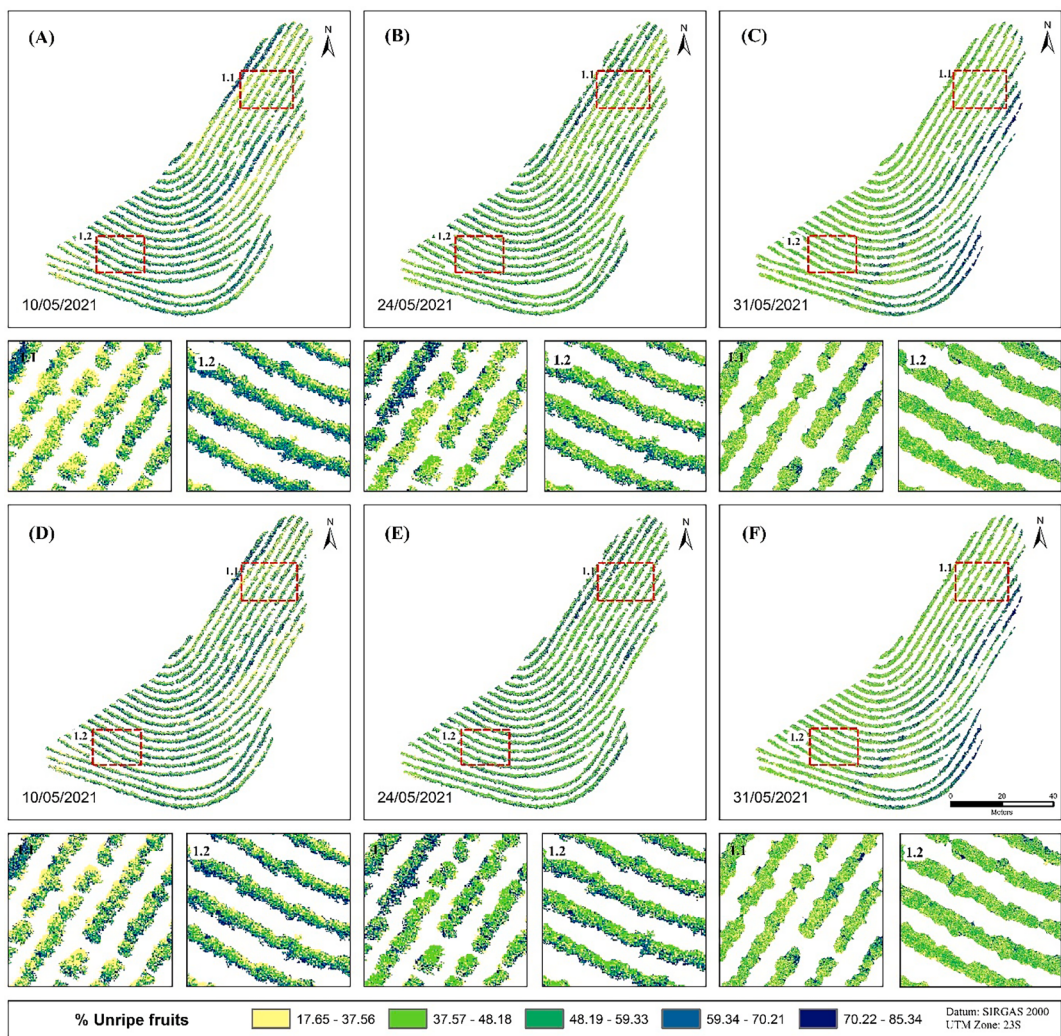


Fig. 10. Spatial variability maps of the fruit ripeness (% unripe fruits) obtained with the random forest models using as predictors the spectral variables (A, B, and C) and the combination of spectral and textural variables (D, E, and F) from field F in 2021. The dashed rectangles identified as 1.1 and 1.2 on the maps represent an amplified view of the crop rows.

Table 5
Temporal evolution of the fruit ripeness extracted from the maps of field A.

Spectral Variables												
Dates	04/05/2021			18/05/2021			24/05/2021			Difference between sampling dates		
Class	Area						18/05-05/05					
(% Unripe fruits)	m ²	%	m ²	%	m ²	%	m ²	%	m ²	%		
17.65-37.56	624.91	26.25	905.92	38.06	939.45	39.47	+281.01	+31.02	+33.53	+3.57		
37.57-48.18	438.32	18.41	302.18	12.69	376.81	15.83	-136.14	-45.05	+74.64	+19.81		
48.19-59.33	608.56	25.56	260.69	10.95	311.48	13.09	-347.87	-133.44	+50.80	+16.31		
59.34-70.21	597.79	25.11	756.29	31.77	664.87	27.93	+158.50	+20.96	-91.42	-13.75		
70.22-85.34	110.88	4.66	155.38	6.53	87.84	3.69	+44.50	+28.64	-67.54	-76.90		

Spectral and Textural Variables										
% Unripe fruits	m ²	%	m ²	%						
17.65-37.56	563.49	23.67	940.45	39.51	934.90	39.27	+376.96	+40.08	-5.55	-0.59
37.57-48.18	532.54	22.37	391.73	16.46	446.54	18.76	-140.81	-35.95	+54.81	+12.28
48.19-59.33	716.15	30.08	335.95	14.11	379.55	15.94	-380.20	-113.17	+43.60	+11.49
59.34-70.21	312.61	13.13	456.89	19.19	428.15	17.99	+144.29	+31.58	-28.75	-6.71
70.22-85.34	255.67	10.74	255.44	10.73	191.33	8.04	-0.23	-0.09	-64.12	-33.51

Table 6

Temporal evolution of the fruit ripeness extracted from the maps of field F.

Spectral Variables											
Dates	10/05/2021		24/05/2021		31/05/2021		Difference between sampling dates				
Class	Area										
(% Unripe fruits)	m ²	%	m ²	%	m ²	%	24/05 – 10/05		31/05 – 24/05		
17.65–37.56	995.63	34.45	1551.35	53.67	2139.77	74.03	+555.72	+35.82	+588.42	+27.50	
37.57–48.18	739.85	25.60	596.42	20.63	430.18	14.88	-143.43	-24.05	-166.24	-38.64	
48.19–59.33	828.07	28.65	484.71	16.77	201.66	6.98	-343.36	-70.84	-283.05	-140.36	
59.34–70.21	203.71	7.05	142.09	4.92	28.74	0.99	-61.62	-43.37	-113.35	-394.46	
70.22–85.34	123.11	4.26	115.80	4.01	90.02	3.11	-7.31	-6.31	-25.78	-28.64	

Spectral and Textural Variables											
% Unripe fruits	m ²	%	m ²	%							
17.65–37.56	804.91	27.85	1437.34	49.73	2077.71	71.88	+632.43	+44.00	+640.37	+30.82	
37.57–48.18	761.54	26.35	663.86	22.97	462.12	15.99	-97.67	-14.71	-201.75	-43.66	
48.19–59.33	943.91	32.66	505.14	17.48	240.41	8.32	-438.77	-86.86	-264.72	-110.11	
59.34–70.21	256.74	8.88	168.11	5.82	21.11	0.73	-88.64	-52.73	-146.99	-696.20	
70.22–85.34	123.27	4.26	115.92	4.01	89.01	3.08	-7.35	-6.34	-26.90	-30.23	

fruit ripeness presents limitations, especially when the majority of the fruits are unripe, which results in high spectral confusion among fruits and leaves leading to underestimation of the fruit ripeness degree. On top of that, the unequal fruit ripeness among trees as well as within a single tree also ends up affecting the fruit ripeness mapping and the decision-making towards the definition of the ideal harvesting time.

Despite these limitations, the approach used in this study provides a framework for integrating field data and the spectral and textural variables derived from UAV imagery to map the fruit ripeness. In addition, the concepts presented here are expected to be consistent regardless of the multispectral sensor, provided that the spatial resolution of the imagery is able to capture the spatial variability of the fruit ripeness. Finally, future research needs to include data from more seasons as well as from several commercial fields to validate the methodology. More importantly, it should focus on developing an automated workflow for image acquisition, variable extraction, and better modeling of the fruit ripeness for practical uses in the future.

5. Conclusion

This study demonstrated that the combined use of spectral and textural variables derived from aerial imagery enhanced the prediction accuracy of the fruit ripeness models compared to the performance obtained using only spectral bands and vegetation indices.

Even though the fruit ripeness varies greatly among trees as well as within a single tree due to multiple coffee blossoms and environmental conditions, the random forest-based models were able to predict and quantify the spatiotemporal changes in fruit ripeness with moderate accuracies for both scenarios. Finally, despite the limitations, this study filled a gap in the literature by developing the fruit ripeness variability maps, which can be used as decision support tools for monitoring and identifying on a temporal scale the area of plants ready and not ready for harvest throughout the season.

Funding

This study was partially financed by the Coordenação de Aperfeiçoamento de Pessoal de Nível Superior (CAPES, Coordination for the Improvement of Higher Education Personnel)-Finance Code 001, and by the Conselho Nacional de Desenvolvimento Científico e Tecnológico (CNPq, The Brazilian National Council for Scientific and Technological Development)-Grant number 144740/2019-2.

CRediT authorship contribution statement

Rodrigo Nogueira Martins: Conceptualization, Formal analysis, Investigation, Methodology, Writing – original draft, Writing – review & editing. **Francisco de Assis de Carvalho Pinto:** Funding acquisition, Project administration, Resources, Writing – review & editing. **Daniel Marçal de Queiroz:** Funding acquisition, Resources, Supervision, Supervision, Writing – review & editing. **Domingos Sárvio Magalhães Valente:** Supervision, Writing – review & editing. **Jorge Tadeu Fim Rosas:** Validation, Visualization, Writing – review & editing. **Marcelo Fagundes Portes:** Validation, Visualization, Writing – review & editing. **Elder Sâñcio Aguiar Cerqueira:** Writing – review & editing.

Declaration of Competing Interest

The authors declare that they have no known competing financial interests or personal relationships that could have appeared to influence the work reported in this paper.

Data availability

Data will be made available on request.

Acknowledgments

We thank the Department of Agricultural Engineering (DEA) of the Universidade Federal de Viçosa for supporting the researchers.

References

- Alvares, C.A., Stape, J.L., Sentelhas, P.C., De Moraes Gonçalves, J.L., Sparovek, G., 2013. Köppen's climate classification map for Brazil. Meteorol. Zeitschrift. <https://doi.org/10.1127/0941-2948/2013/0507>.
- Bernardes, T., Moreira, M.A., Adami, M., Giarolla, A., Rudorff, B.F.T., 2012. Monitoring biennial bearing effect on coffee yield using MODIS remote sensing imagery. Remote Sens. <https://doi.org/10.3390/rs4092492>.
- Breiman, L., 2001. Random forests. Mach. Learn. <https://doi.org/10.1023/A:1010933404324>.
- Cannell, M.G.R., 1975. Crop physiological aspects of coffee bean yield: a review. J. Coffee Res. 1.
- DadrasJavan, F., Samadzadegan, F., Seyed Pourazar, S.H., Fazeli, H., 2019. UAV-based multispectral imagery for fast Citrus Greening detection. J. Plant Dis. Prot. <https://doi.org/10.1007/s41348-019-00234-8>.
- DaMatta, F.M., Ronchi, C.P., Maestri, M., Barros, R.S., 2007. Ecophysiology of coffee growth and production. Brazilian J. Plant Physiol. <https://doi.org/10.1590/S1677-04202007000400014>.
- Dos Reis, A.A., Werner, J.P.S., Silva, B.C., Figueiredo, G.K.D.A., Antunes, J.F.G., Esquerdo, J.C.D.M., Coutinho, A.C., Lamparelli, R.A.C., Rocha, J.V., Magalhães, P.S., G., 2020. Monitoring Pasture Aboveground Biomass and Canopy Height in an

- Integrated Crop-Livestock System Using Textural Information from PlanetScope Imagery. *Remote Sens.* <https://doi.org/10.3390/rs12162534>.
- Fitzgerald, G.J., Rodriguez, D., Christensen, L.K., Belford, R., Sadras, V.O., Clarke, T.R., 2006. Spectral and thermal sensing for nitrogen and water status in rainfed and irrigated wheat environments. *Precis. Agric.* <https://doi.org/10.1007/s11119-006-9011-z>.
- Fu, Y., Yang, G., Li, Z., Song, X., Li, Z., Xu, X., Wang, P., Zhao, C., 2020. Winter wheat nitrogen status estimation using uav-based rgb imagery and gaussian processes regression. *Remote Sens.* 12, 1–27. <https://doi.org/10.3390/rs12223778>.
- Fu, Y., Yang, G., Song, X., Li, Z., Xu, X., Feng, H., Zhao, C., 2021. Improved estimation of winter wheat aboveground biomass using multiscale textures extracted from UAV-based digital images and hyperspectral feature analysis. *Remote Sens.* 13, 1–22. <https://doi.org/10.3390/rs13040581>.
- Gitelson, A.A., Kaufman, Y.J., Merzlyak, M.N., 1996. Use of a green channel in remote sensing of global vegetation from EOS- MODIS. *Remote Sens. Environ.* [https://doi.org/10.1016/S0034-4257\(96\)00072-7](https://doi.org/10.1016/S0034-4257(96)00072-7).
- Haboudane, D., Miller, J.R., Pattee, E., Zarco-Tejada, P.J., Strachan, I.B., 2004. Hyperspectral vegetation indices and novel algorithms for predicting green LAI of crop canopies: Modeling and validation in the context of precision agriculture. *Remote Sens. Environ.* <https://doi.org/10.1016/j.rse.2003.12.013>.
- Haralick, R.M., Shanmugam, K., Dinstein, I., 1973. Textural Features for Image Classification. *IEEE Trans. Syst. Man. Cybern. SMC-3*, 610–621. <https://doi.org/10.1109/TSMC.1973.4309314>.
- Herwitz, S.R., Johnson, L.F., Dunagan, S.E., Higgins, R.G., Sullivan, D.V., Zheng, J., Lobitz, B.M., Leung, J.G., Gallmeyer, B.A., Aoyagi, M., Slye, R.E., Brass, J.A., 2004. Imaging from an unmanned aerial vehicle: Agricultural surveillance and decision support. *Comput. Electron. Agric.* <https://doi.org/10.1016/j.compag.2004.02.006>.
- Hijmans, R., Etten, J., Van, ... J.C.-R., 2015, U., 2012. Package "raster." h64-50-233-100. mdsnwi.tisp.static.
- Johnson, L.F., Herwitz, S.R., Lobitz, B.M., Dunagan, S.E., 2004. Feasibility of monitoring coffee field ripeness with airborne multispectral imagery. *Appl. Eng. Agric.*
- Kuhn, M., 2008. caret Package. *J. Stat. Softw.*
- Liu, Y., Liu, S., Li, J., Guo, X., Wang, S., Lu, J., 2019. Estimating biomass of winter oilseed rape using vegetation indices and texture metrics derived from UAV multispectral images. *Comput. Electron. Agric.* 166, 105026 <https://doi.org/10.1016/j.compag.2019.105026>.
- Louzada Pereira, L., Carvalho Guarçoni, R., Soares Cardoso, W., Córrea Taques, R., Rizzo Moreira, T., da Silva, S.F., Schwengber ten Caten, C., 2018. Influence of Solar Radiation and Wet Processing on the Final Quality of Arabica Coffee. *J. Food Qual.* <https://doi.org/10.1155/2018/6408571>.
- Marin, D.B., Ferraz, G.A. e S., Guimaraes, P.H.S., Schwerz, F., Santana, L.S., Barbosa, B.D. S., Barata, R.A.P., Faria, R. de O., Dias, J.E.L., Conti, L., Rossi, G., 2021. Remotely Piloted Aircraft and Random Forest in the Evaluation of the Spatial Variability of Foliar Nitrogen in Coffee Crop. *Remote Sens.* 13, 1471. <https://doi.org/10.3390/rs13081471>.
- Martinez, H.E.P., Poltronieri, Y., Farah, A., Perrone, D., 2013. Zinc supplementation, production and quality of coffee beans. *Rev. Ceres* 60, 293–299. <https://doi.org/10.1590/S0034-737X20130002000020>.
- Merzlyak, M.N., Gitelson, A.A., Chivkunova, O.B., Rakitin, V.Y., 1999. Non-destructive optical detection of leaf senescence and fruit ripening. *Physiol. Plant.* 106, 135–141.
- Meyer, D., Dimitriadou, E., Hornik, K., Weingessel, A., Leisch, F., Chang, C.-C., Lin, C.-C., 2019. Package "e1071". R News.
- Meyer, G.E., Hindman, T., 1998. Machine Vision Detection Parameters for Plant Species Identification, in: SPIE Conference on Precision Agriculture and Bioloical Quality. Boston, Massachusetts, pp. 327–335.
- Nogueira Martins, R., de Carvalho Pinto, F. de A., Marçal de Queiroz, D., Magalhães Valente, D.S., Fim Rosas, J.T., 2021. A Novel Vegetation Index for Coffee Ripeness Monitoring Using Aerial Imagery. *Remote Sens.* <https://doi.org/10.3390/rs13020263>.
- R Core Team, 2021. R: A Language and Environment for Statistical Computing. Austria, Vienna.
- Rosas, J.T.F., de Carvalho Pinto, F. de A., de Queiroz, D.M., de Melo Villar, F.M., Magalhães Valente, D.S., Nogueira Martins, R., 2021. Coffee ripeness monitoring using a UAV-mounted low-cost multispectral camera. *Precis. Agric.* 19. <https://doi.org/10.1007/s11119-021-09838-3>.
- Rosas, J.T.F., de Carvalho Pinto, F. de A., Queiroz, D.M. de, de Melo Villar, F.M., Martins, R.N., Silva, S. de A., 2020. Low-cost system for radiometric calibration of UAV-based multispectral imagery. *J. Spat. Sci.* 00, 1–15. <https://doi.org/10.1080/14498596.2020.1860146>.
- Rouse, J.W., Haas, R.H., Schell, J.A., Deeering, D., 1973. Monitoring vegetation systems in the Great Plains with ERTS (Earth Resources Technology Satellite)., in: Third Earth Resources Technology Satellite-1 Symposium.
- Schumacher, P., Mislimshoeva, B., Brenning, A., Zandler, H., Brandt, M., Samimi, C., Koellner, T., 2016. Do red edge and texture attributes from high-resolution satellite data improve wood volume estimation in a semi-arid mountainous region? *Remote Sens.* 8, 1–19. <https://doi.org/10.3390/rs8070540>.
- Silva, S. de A., de Queiroz, D.M., Pinto, F. de A.C., Santos, N.T., 2014. Coffee quality and its relationship with Brix degree and colorimetric information of coffee cherries. *Precis. Agric.* <https://doi.org/10.1007/s11119-014-9352-y>.
- Silva, T.V., Hubinger, S.Z., Gomes Neto, J.A., Milori, D.M.B.P., Ferreira, E.J., Ferreira, E. C., 2017. Potential of Laser Induced Breakdown Spectroscopy for analyzing the quality of unroasted and ground coffee. *Spectrochim. Acta - Part B At. Spectrosc.* 135, 29–33. <https://doi.org/10.1016/j.sab.2017.06.015>.
- Soares, J.V., Rennó, C.D., Formaggio, A.R., Yanasse, C.D.C.F., Frery, A.C., 1997. An investigation of the selection of texture features for crop discrimination using SAR imagery. *Remote Sens. Environ.* 59, 234–247. [https://doi.org/10.1016/S0034-4257\(96\)00156-3](https://doi.org/10.1016/S0034-4257(96)00156-3).
- Venables, W. N., Ripley, B. D. 2002. Modern Applied Statistics with S. 4th edition. SpringerVerlag, New York. Available at: <<http://www.stats.ox.ac.uk/pub/MASS4>>.
- Wang, F., Yi, Q., Hu, J., Xie, L., Yao, X., Xu, T., Zheng, J., 2021. Combining spectral and textural information in UAV hyperspectral images to estimate rice grain yield. *Int. J. Appl. Earth Obs. Geoinf.* 102, 102397 <https://doi.org/10.1016/j.jag.2021.102397>.
- Wood, E.M., Pidgeon, A.M., Radloff, V.C., Keuler, N.S., 2012. Image texture as a remotely sensed measure of vegetation structure. *Remote Sens. Environ.* 121, 516–526. <https://doi.org/10.1016/j.rse.2012.01.003>.
- Zheng, H., Cheng, T., Li, D., Zhou, X., Yao, X., Tian, Y., Cao, W., Zhu, Y., 2018. Evaluation of RGB, color-infrared and multispectral images acquired from unmanned aerial systems for the estimation of nitrogen accumulation in rice. *Remote Sens.* 10 <https://doi.org/10.3390/rs10060824>.
- Zheng, H., Cheng, T., Zhou, M., Li, D., Yao, X., Tian, Y., Cao, W., Zhu, Y., 2019. Improved estimation of rice aboveground biomass combining textural and spectral analysis of UAV imagery. *Precis. Agric.* 20, 611–629. <https://doi.org/10.1007/s11119-018-9600-7>.
- Zvoleff, A., 2020. Glcm: Calculate Textures from Grey-Level Co-Occurrence Matrices (GLCMs).